RSC Advances

ROYAL SOCIETY OF CHEMISTRY

www.rsc.org/advances

Davydov Splitting in Cadmium Vacancy Emission, Ferromagnetism and Photosensitivity in Manganese incorporated CdS nanocrystals

Balaji Sambandam[a], Thangavelu Muthukumar[b], Sonachalam Arumugam[c] P. L. Paulose[d] and Periakaruppan T Manoharan[a]*

[a] Department of Chemistry, Indian Institute of Technology/Madras, Chennai, 600 036, India, [b]Department of Bio Products, Central Leather Research Institute, Adyar, Chennai, 600 025, India, [c]Centre for High Pressure Research, School of Physics, Bharathidasan University, Tiruchirappalli, 620 024, India and [d] Department of Condensed Matter and Physics, Tata Institute of Fundamental Research, Homi Bhabha Road, Colaba, Mumbai, India

Abstract

Nanocrystals of CdS/Mn^{2+} synthesized using sodiumlaurylsulphate (SLS) surfactant and two ligands, butylenediamine (BD) and propylenediamine (PD) of differing lengths, show a dominant presence of hexagonal phase. The increasing [Mn^{2+}] in the CdS/Mn^{2+} crystals from BD medium leads to a red shift of the band gap absorption with increasing intensity while these optical properties are reversed in CdS/PD crystals. Such changes can be explained by the switching of the randomly blinking nanocrystals into coherently emitting nanocrystals. The photoluminescence of CdS/Mn^{2+} materials with similarities and differences between SLS/BD and SLS/PD media exhibits two emissions, one at 2.25 eV due to cadmium ion vacancies exhibiting Davydov type splitting from neighbouring Cd^{2+}-Cd^{2+} vacancies and other around 2.18 eV from manganese d-d emission. Addition of Mn^{2+} leads to a decrease in the intensity of vacancy emission and increase in d-d emission due to occupation by manganese in cadmium vacant sites. Interestingly, SLS/PD medium creates more defects in CdS nanocrystals than SLS/BD medium. The CdS/Mn^{2+} nanocrystals made from SLS/BD medium exhibit weak ferromagnetism in pre-annealed samples, becoming stronger after annealing while the preannealed samples from SLS/PD origin have the simultaneous presence of both superparamgnetism and ferromagnetism which turns to complete ferromagnetism on annealing. An attempt has also been made to compare the various properties of nanomaterials made as a function of two surfactants and three diamines of differing lengths. These nanoparticles are in the size range of 10 to 15 nm. A simple photo-resistance experiment on CdS and carbon nanoparticles based heterostructure reveal its photosensitivity.

1. Introduction

It is now well known that the electronic properties of a semiconductor having its dimensions reduced to a few nanometers can undergo drastic changes. This progressive transition from bulk to molecular-like behavior has been a subject of extensive investigations and is now well understood in terms of quantum confinement.[1] Most of them were achieved on II-VI group compounds, monodispersed nanoparticles of which

can be well controlled by proper synthetic procedures.

Diluted magnetic semiconductors (DMS) are ternary alloys in which cations of semiconductor matrix are randomly substituted by magnetic ions that exhibit unique physical and chemical properties due to the confinement effects.[1,2] Specially, transition metals ions doped compounds have been extensively investigated as typical DMS because of their wide band gaps and outstanding opto-magneto properties.[3-5] Bulk II-VI semiconductors doped with transition metal ions may be of special interest since they are already well known as good luminophores, especially in systems of the kind, CdS/ZnS:Mn.[6] Such compounds as nanoparticles can be synthesized with the main purpose of studying the effect of quantum confinement on the luminescence properties.[7,8] CdS is itself considered as a typically important phosphor both in basic and applied science; consequently the changes in molecular and electronic structure, optical emission and absorption processes caused by introducing manganese while creating $Cd_{1-x}Mn_xS$ make them highly attractive candidates for opto-magnetic investigations. [9,10]

Although there are a large numbers of publications involving Mn-based semiconductors, specifically $Cd_{1-x}Mn_xS$, we have investigated the properties of such nanocrystals with various Mn compositions with our method of synthesis and attempted to understand their new or modified properties. Our own experience suggests[5,11-13] that using different kinds of diamine ligands in the medium of differing surfactants can alter the structural morphology which in turn allow us to tune their optical and magnetic properties.

This work is important since we have earlier reported[11] with the same anionic surfactant, Sodium Lauryl Sulfate (SLS), used also in this work and a smaller ligand, ethylenediamine (ED) based CdS/Mn^{2+} nanorods with an interesting physical property of "Davydov splitting"[11] in the photoluminescence spectra arising from surface doping by guest Mn^{2+} ions. The physical properties such as absorption, emission and magnetism change dramatically by the increase of the diamine ligand chain length from ED to intermediate sized propylenediamine (PD) and then the larger sized butylenediamine (BD). Yet another important set of changes in property of these nanomaterials is caused

by changing the surfactant but keeping the same ligand. Our earlier work with the use of CTAB (Cetyltrimethylammoniumbromide) surfactant with BD leads to the formation of 100% cubic morphology which could be converted to pure hexagonal form without any harsh treatment but by simple addition of manganous ions.[12] In the present work we have attempted to synthesize such nanoparticles with the use of SLS surfactant and the two ligands BD and PD with differing chain length both being larger than the earlier used ED ligand. Most importantly we noted the large presence of cadmium ion vacancy leading to photoluminescence with Davydov splitting, this time such splitting originates from the host ion unlike the guest ion from our earlier work. What is even more amazing is the differential effect of addition of magnetic ion like manganese on the SLS/PD and SLS/BD assisted CdS/Mn^{2+} and resultant changes in light absorption and emission, magnetic and photovoltaic properties. The latter property indicates that these heterostructures with carbon nanoparticles (CNP) could be used as thermistors. Finally a comparative account of the properties as a function of surfactant and ligands has been made. It must be borne in mind that preparatory methods were kept identical but for change of ligands and surfactants to allow a critically valid comparison.

2. Experimental

2.1 Synthesis of CdS and CdS/Mn^{2+} nanocrystals

3 g of sodium lauryl sulfate (SLS) was dissolved in 5 ml ultra pure distilled water. To this 0.308 g of cadmium nitrate tetrahydrate and 10 ml 1, 4-diaminobutane (BD) were added and the resultant solution kept for refluxing with constant stirring. During the refluxing, 0.228 g thiourea was (dissolved in minimum amount of distilled water) added and the refluxing continued for 12 hrs with 120 ºC. The appearance of pale yellow precipitate indicates the formation CdS nanocrystals. The precipitate was washed with distilled water and methanol several times. Finally the product was thoroughly dried in the oven at 60 degrees for 3 hrs. The same procedure has been adopted for 0.1, 0.5, 1.0, and 5.0 mole % Mn^{2+} loaded CdS nanocrystals with appropriate amounts of cadmium and manganese salts. An exactly similar procedure was adopted using the ligand 1,3-diaminopropane (PD) instead of BD.

2.2 Instruments

The XRD patterns were recorded in a Bruker Discover D8 powder X-ray diffractometer using Cu-K_α as a radiation source. The optical properties were studied by UV-Vis (Varian CARY 5E), and fluorescence (JOBIN YUON Fluorolog-3-11) spectroscopy. Electron Paramagnetic Resonance (EPR) measurements were made using Bruker X-band CW EPR both at room temperature (300 K) and liquid nitrogen temperature (77 K) and Bruker ELEXSYS 500 (*Bruker BioSpin*) for 10 K. High resolution TEM studies were conducted using a JEOL JEM 3010 operated at 300 kV. Energy Dispersive Spectrum (EDS) pattern was recorded using a Philips CM12 TEM attached analyzer. Magnetic measurements on SLS/BD samples were made with the use of 9T -PPMS with VSM & helium reliquifier, Quantum Design, USA down to 8 K. Inductively Coupled Plasma-Optical Emission Spectrometry (ICP-OES), Perkin Elmer Optima 5300 DV, measurements were made to calculate manganese concentration. The dc magnetic susceptibility measurements on SLS/PD samples were carried out in the temperature interval 1.8–330 K, using a commercial superconducting quantum interference device (SQUID) magnetometer from Quantum Design, USA. The samples were cooled to 1.8 K in zero external magnetic field and then the required magnetic field was turned on to record zero-field cooled data.

3. Results and Discussion

3.1 Presence of both cubic and hexagonal morphologies, the latter being dominant, independent of [Mn^{2+}]

Fig. 1 shows the powder XRD patterns for SLS/BD and SLS/PD assisted pure and manganese doped CdS nanocrystals. It is well known that both pure and doped CdS nanocrystals exhibit either pure cubic or hexagonal phases or different combinations of both though the latter may dominate over the former in many cases since the cubic structure is metastable. The average particle size from XRD measurement for these SLS/BD and SLS/PD samples found to be in the range of 9-10.5 nm and 12-14 nm respectively and values of all samples are given in Electronic Supplementary Information

(ESI Table 1). Though the XRD patterns look similar to the cubic phase (Fig. 1a and 1b), the presence of hexagonal phase is less dominant in SLS/BD as revealed by the presence of the peaks around 25-30˚ for the planes of (100), (002) and (101) and another peak around 48˚, which is the characteristic (103) peak of the hexagonal phase. But the SLS/PD assisted samples exhibit clear resolution of the (100), (002) and (101) and (103) hexagonal planes making it more dominant; however, it is again suspected to have a small percentage of cubic phase present in the sample. The poorer resolution of the SLS/BD is expected to have a lesser percentage of the hexagonal phase, both needing a deeper analysis of the mixed phases. Thus it is necessary to perform the deconvolution of the peaks to identify the quantum of each component in mixed crystals. The percentage of both components has been calculated by Short and Steward method.[14] A proper deconvolution[5,12,14] (explained in ESI) of the XRD pattern (given in ESI Fig. 1) indicates a mixture of phases. But it is surprising to note that increasing the [Mn^{2+}] does not seem

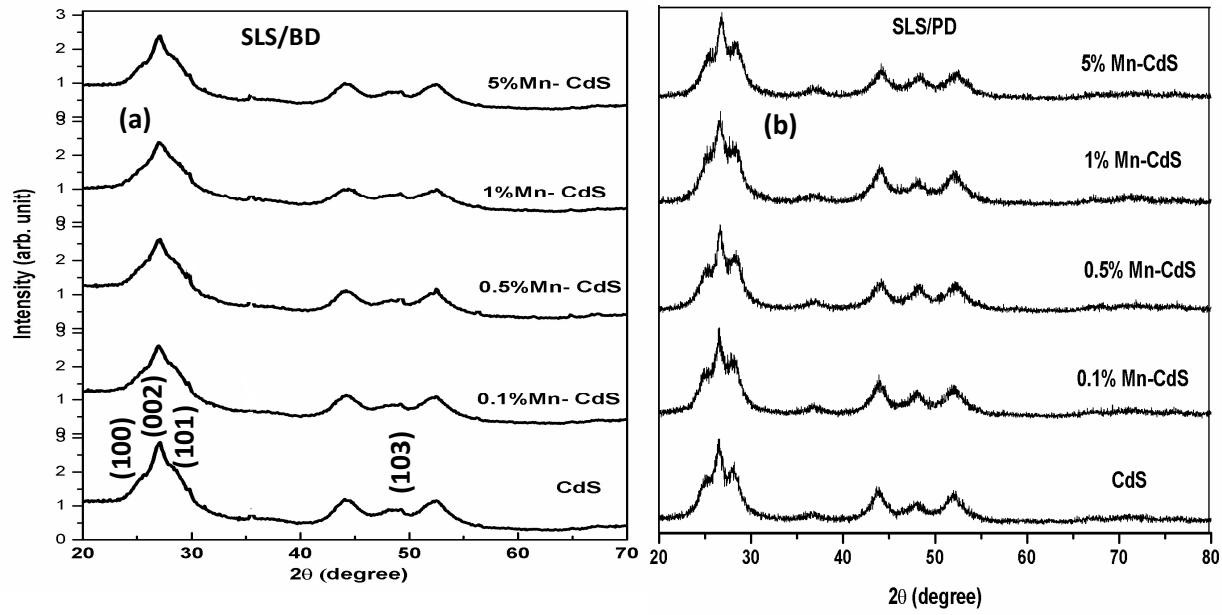

Fig. 1: Powder XRD pattern of SLS surfactant assisted (a) butylenediamine (b) propylenediamine mediated pure and manganese doped CdS nanocrystals.

to influence the percentage composition of hexagonal and cubic morphologies which remain constant during the addition of manganese ions up to 5% ; the percentage

composition of the two phases is listed in Table 1. While the smallest ligand i.e., ethylenediamine produces a purely (100%) hexagonal material (10) both the propylenediamine and butylenediamine creates a mixture of species, with 90% and 81% of the hexagonal species respectively, all three of them in presence of the same SLS surfactant. Hence the percentage composition

Table 1: A comparative account of morphology compositions from powder XRD data using Short and Steward method with SLS/BD, SLS/PD and SLS/ED and CTAB/BD

Surfactant/Ligand	% of Cubic	% of Hexagonal
SLS/ED (0-5% Mn^{2+})	Nil	100 Ref. 11
SLS/PD (0-5% Mn^{2+})	~10	90 (This work)
SLS/BD (0-5% Mn^{2+})	19	81 (This work)
CTAB/BD(0%Mn^{2+})	100$^{\$}$	Nil Ref. 12

$^{\$}$ Addition of 5% Mn^{2+} facilitates total conversion to hexagonal

seems to be dictated by the length of the ligands. Increase in the length of the ligand seems to facilitate the part conversion from hexagonal to cubic. It is, however, surprising to note that the CTAB/BD[12] provides 100% cubic morphology for pure CdS nanopaticles, which can, however, be completely converted to the hexagonal form by the addition of 5% Mn^{2+} without any harsh treatment like high temperature heating, high pressure, etc. Despite the use of common ligands in both cases, the formations of micelles of the two different surfactants are different and this should have played a key role for diverse properties of the materials. Similarly a simple change of ligand from ED to PD and BD keeping the same surfactant, i.e. SLS converts the CdS/Mn^{2+} from 100% hexagonal to mixed phases. Here again, the length of the ligand plays a role. It is also interesting to note that the largest of the three ligands drives the CdS nanocrystals towards the cubic morphology in SLS medium though incomplete while with the same ligand the CTAB achieves 100% metastable cubic morphology. These subtle changes require to be

understood in future.

3.2 Differential Scanning Calorimetry confirms the presence of Cubic and Hexagonal phases in CdS/Mn^{2+} from both SLD/BD and SLS/PD media

The percentage of cubic and hexagonal phases have been identified and quantified by a simple method proposed earlier by us.[5] In order to calculate the exact percentage of cubic and hexagonal phases in a given mixture, we need a pure cubic sample and this has been taken from a surfactant/amine (CTAB/BD) assisted CdS nanocrystals without manganese as we normally denoted by CTAB/BD/0% Mn^{2+}/CdS from our earlier work.[12] This has been taken as a reference or base material. The DSC depicts the nature of DSC curves for SLS/BD and SLS/PD assisted with and without manganese doped CdS nanocrystals. It is important to compare these curves with a real cubic (100%) curve of CTAB/BD/0%Mn^{2+}/CdS in order to calculate the exact percentages of cubic and hexagonal phases. The measurements are performed under the same condition as for CTAB/BD/0%Mn^{2+}/CdS nanocrystals[5] (N_2 atmosphere; same quantity; same temperature step width, etc.). In the case of CTAB/BD assisted 0% Mn^{2+}/CdS, the cubic to hexagonal transition (phase conversion) is from 100% cubic component alone. On the other hand all SLS/BD and SLS/PD assisted samples are naturally mixed with both cubic and hexagonal phases (see XRD discussion *vide infra* and Table 1) the exothermic peak arises only from the cubic component of the mixture and not from thermodynamically stable hexagonal component. Thus by measuring the area under the curve in the DSC measurement, the percentage of cubic component has been calculated and hence the hexagonal component by simple subtraction. There is excellent agreement between the results from XRD and DSC. In a similar fashion the percentage of cubic and hexagonal components for SLS/PD assisted samples has been calculated. The calculated values and DSC profile for these materials as given in ESI Fig. 2 and ESI Table 2.

3.3 Red and blue shifted Band gap absorptions in SLS/BD and SLS/PD assisted CdS/ Mn^{2+} nanocrystals: increase of energy shift related to decrease of chain length.

Solid-state optical absorption spectra of SLS/BD and SLS/PD assisted undoped and manganese doped CdS nanocrystals are shown in Fig. 2. The absorption maximum

(λ_{max}) around 492- 510 nm (2.52 to 2.43 eV) decides its band gap energy. It is evident that CdS shows red shifted absorption in SLS/BD assisted samples as a function of increasing manganese concentration. However, the optical absorption of CdS/Mn^{2+}

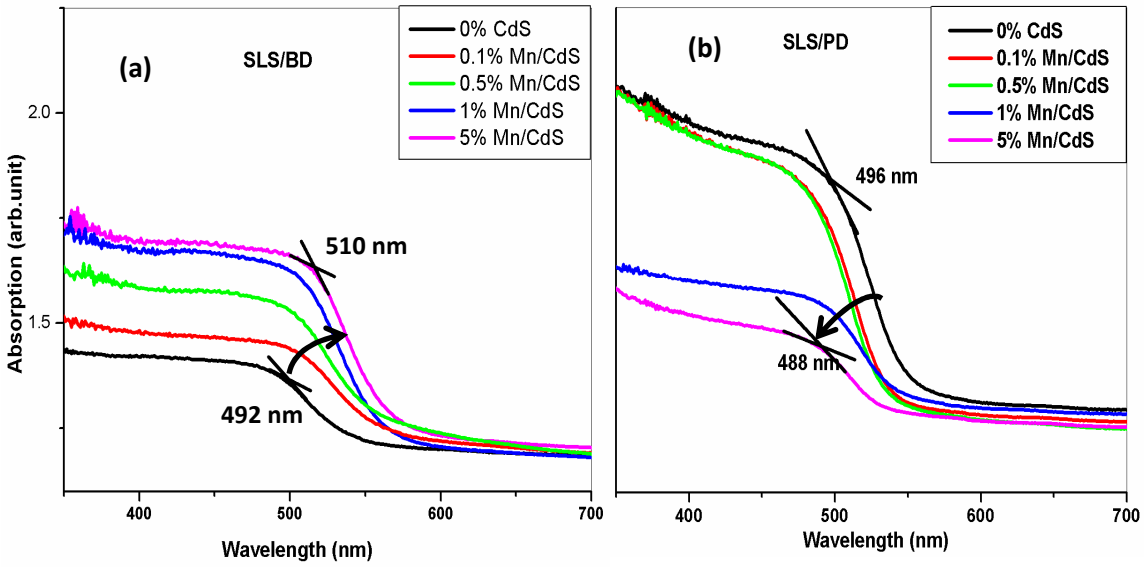

Fig. 2: Solid-state optical absorption spectra of (a) SLS/BD and (b) SLS/PD assisted undoped and manganese doped CdS nanocrystals.

nanoparticles in SLS/PD medium suffers blue shift in its band gap absorption from 496 to 488 nm (2.50 to 2.54 eV) revealing a weak quantum confinement. It is similarly interesting that with the smallest sized ligand i.e. ED it is with a much higher blue shift (2.59 to 2.70 eV*)*. While in most CdS materials including SLS/ED and SLS/PD origin the band gap absorption takes place in the region of 460-480 nm (2.59 -2.7 eV) during blue shift, our absorption peak in SLS/BD occurs at 480-510 nm, a case of red shifted absorption, both being part of band gap absorption with 480 nm being the centre of the band gap. On the other hand, we observed a clear blue shift in the optical absorption as a function of Mn^{2+} input for the same ligand including that from a different surfactant, i.e., CTAB/BD.[12] However, this blue shift observation strongly depends on the particle size of the CdS nanocrystals. This kind of differing energy shift, both blue and red shift from a higher value of 2.7 eV to a lower value of 2.43 eV or in reverse can be explained by the switching of the randomly blinking nanocrystals into a coherently emitting NCs[15] and

possibly with differing compositions due to cubic and hexagonal morphologies. The blinking and non-blinking actually has a relation to the various band gap levels.

The second important observation relates to the change in the intensity of band gap absorption during the increased intake of Mn^{2+}; while BD assisted CdS/Mn^{2+} showed an increase in intensity the PD assisted CdS/Mn^{2+} revealed a decrease. Increase in the intensity of the band gap absorption with an accompanying decrease in band gap energy as a function of [Mn^{2+}] in the case of the former and the reverse situation in the latter can be attributed to the magnitude of VB-CB separation, more energy separation means less transition probability. In addition an increase in energy shift and hence the band gap (ESI Fig.3) seems to be proportional to a decrease in ligand chain length as seen from the longest BD to the intermediate PD to the shortest ED.

3.4 Davydov Split Photoluminescence (PL) from V_{Cd} and differing Characteristics of d-d emission due to change of Surfactant and ligand

In contrast to the use of the smallest ligand (ED) in SLS medium showing a large number of emissions[11], the PL of CdS/ Mn^{2+} nanocrystals made from the larger PD and BD ligands is a simple case of two emission process (Fig. 3) when excited by 300 nm wavelength. The one at 2.25 eV corresponds to cadmium vacancies emission[5] denoted as $V_{Cd,}$ whereas the other emission around 2.18 eV is the characteristic forbidden d-d emission of manganese due to $^4T_1 \rightarrow {}^6A_1$ energy level.[16-18]

3.4.1 Davydov splitting in SLS/BD assisted CdS/Mn^{2+}

The energy PL spectrum of pure BD assisted CdS before manganese addition shows a pure Gaussian line shape only due to Cadmium vacancies (V_{cd}).[5] However on the addition of manganese a low energy shoulder shows up due to manganese d-d emission.[16-18] The PL spectra of BD assisted CdS/Mn, as shown in Fig. 3 have been deconvoluted to bring out the parameters of the two emissions. The intensity as well as the line width (FWHM) of the V_{Cd} emission centred at 551 nm (2.25 eV) gradually decrease during the addition of manganese as the loaded ions being placed in the position of cadmium vacancies. However, this peak position of this vacancy emission remains unaltered at 2.25 eV though the measured FWHM continuously decreases along with a simultaneous reduction in its intensity on increasing [Mn^{2+}]. The data on line width and

peak intensity and of cadmium and manganese emissions are shown in Table 2. On the other hand, the d-d emission intensity of manganese around ~ 2.18 eV increases on increasing [Mn^{2+}]. In addition this emission peak position shows a small red shift in wavelength as a function of its concentration i.e., towards lower energy from 2.18 eV for 0.1% Mn^{2+}/CdS to 2.14 eV for 5% Mn^{2+}/CdS nanocrystals in conformity with a similar red shift in the band gap absorption in the UV-DRS. The low energy shift by Mn^{2+} indicates its occupying the vacant Cd^{2+}, thereby proving the shift in the band gap absorption and the corresponding effect on the d-d emission. The presence of manganese d-d emission has been corroborated by EPR measurements (*vide infra)*; all the measured PL parameters are given in Table 2. We observed similar linewidth/intensity change in our earlier reported work on CdS/ Mn^{2+} nanocrystals made in the medium of CTAB/PD.[5]

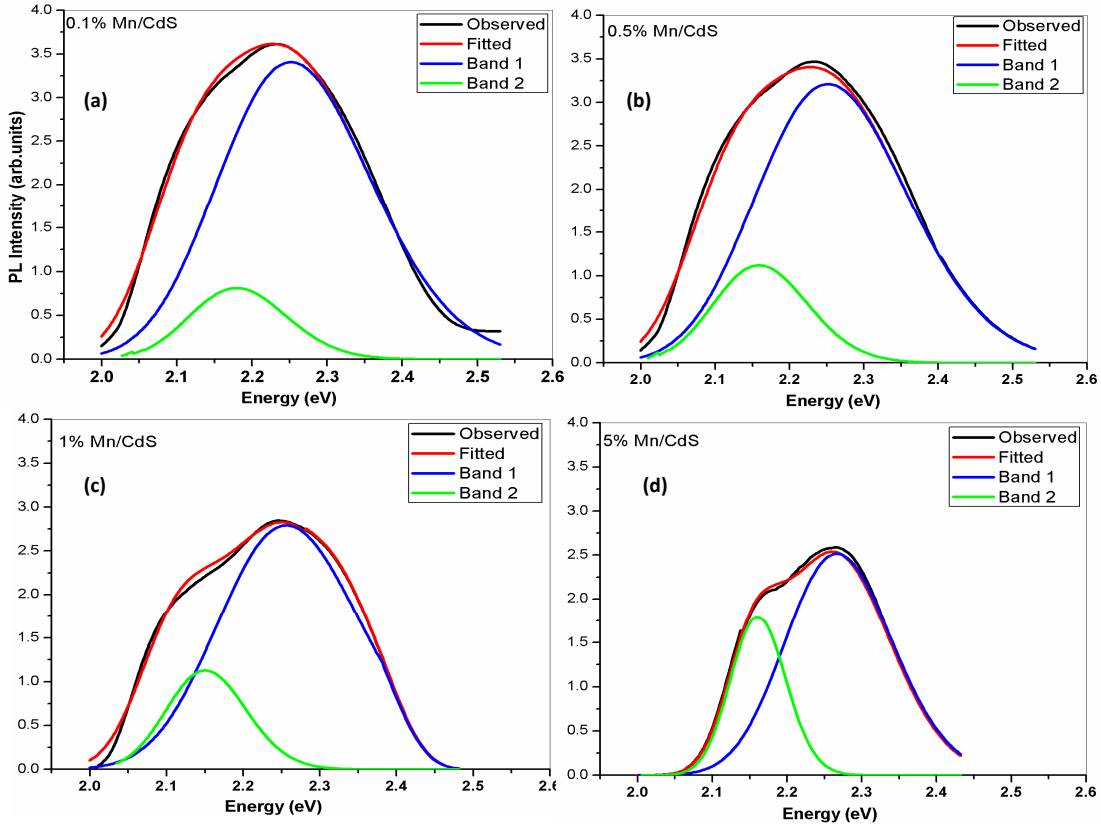

Fig. 3. Deconvoluted PL emission for (a) 0.1, (b) 0.5, (c) 1 and (d) 5% Mn^{2+}/CdS nanocrystals from SLS/BD medium; V_{cd} emission (band 1); d-d emission (band 2)

Table 2. PL intensity profile for V_{Cd} and Mn d-d emissions for 0.1% to 5% Mn^{2+}/CdS nanocrystals from SLS/BD medium

System	Peak position (eV)	Peak width (cm^{-1})	Peak amplitude (a.u)	Peak intensity (a.u)
Pure CdS V_{Cd}	2.25	1992	3.57	3555
0.1% V_{Cd}	2.25	1978	3.42	3382
Mn^{2+}	2.178	1195	0.75	448
0.5% V_{Cd}	2.25	1927	3.22	3102
Mn^{2+}	2.168	1119	1.1	615
1% V_{Cd}	2.25	1820	2.76	2512
Mn^{2+}	2.159	1098	1.2	658
5% V_{Cd}	2.25	1351	2.50	1689
Mn^{2+}	2.140	758	1.82	690

3.4.2 Davydov Splitting of V_{Cd} emission:

First of all, the source of this single broad yellow-green emission (551 nm; 2.25 eV) independent of manganese concentration is from cadmium-vacancy-related defect states (V_{Cd}). Hence, an explanation is needed not only for the sharp decrease in its line width but also for the increase in the d-d emission intensity as a function of [Mn^{2+}] both of which seem to be related to each other. The EDAX profile (Fig. 9) on the atomic concentration of cadmium in CdS nanocrystals shows it to be much less than that of sulfur suggesting both the possibility of a large number of Cd^{2+} vacancies and consequently the V_{Cd} mechanism for the first emission. Such vacancies will be statistically distributed either close to each other, as homometallic Cd^{2+}-Cd^{2+} vacant pairs or as isolated single Cd^{2+} vacancies. Any vacancy emission from the former will lead to Davydov type of interaction[5,11] making the PL emission broader (see below for proof) while the emission from the isolated non-neighbor site will be sharper. The former will be more dominant in manganese-free CdS as seen from its large line width of 1992 cm^{-1}.

Line width reduction in this 2.25 eV emission during the initial addition of Mn^{2+} can be attributed to the reduction in the number of cadmium vacancy intersite interactions

because of the partial occupation of Cd^{2+} vacant sites by Mn^{2+} leading to the formation of heterometallic pairs *viz* "vacant Cd^{2+}- filled Mn^{2+}"; this single occupation will lead to decreased line width due to a decrease in the number of such homometallic cadmium vacancy sites resulting in the loss of Davydov splitting and hence the sharpening of the emission from Cd vacancy sites.

In the current deconvoluted emission profile of CdS/Mn^{2+} (Fig. 4) an orange d-d emission located at 580 nm (2.1 eV) is interpreted as already mentioned as due to the well known $^4T_1 \rightarrow {}^6A_1$ transition of the isolated Mn^{2+} ions. Also we observed a minor red shift in $\lambda_{max.}$ More luminescent centers of this kind are formed on increasing $[Mn^{2+}]$ ion either from the Cd^{2+}-Mn^{2+} or due to the occupation of isolated Cd^{2+} vacancy by Mn^{2+} which contributes to increase in the intensities of both d-d emission and EPR signal I with resolved manganese hyperfine lines (*vide infra*). This emission is distinctly observable in all concentration of Mn^{2+}. Furthermore, in contrast to the 550 nm emission, the manganese d-d emission increases in intensity along with a decreasing line width on increasing $[Mn^{2+}]$. The reduction in the line width and increase in amplitude on increasing $[Mn^{2+}]$ may be interpreted as follows: the initial filling of V_{Cd} present in the form of homometallic Cd-Cd vacant sites, (causing possible Davydov interaction) will form Cd-Mn pairs in which Mn^{2+} ion may oscillate between these two initially vacant but closer Cd sites leading to a motional or Doppler broadening which will cease when both homometallic sites get occupied by the dopant ions, causing a reduction in the line width. However, further addition of Mn^{2+} will occupy on one hand the already created Cd-Mn sites to form homometallic Mn^{2+}-Mn^{2+} dimers and on the other hand the sites of uncoupled isolated Cd^{2+} and also the left over homometallic Cd-Cd vacant sites to produce some more heterometallic Cd^{2+}-Mn^{2+} pairs. The first one will give rise to Mn-Mn exchange coupled species leading to spin-orbit quenching of the d-d emission but the latter two additions will lead to increased intensity for the d-d emission. The first one causes exchange coupled dimers leading to the broad EPR line(signal II) and the latter Cd-Mn pairs or isolated Mn^{2+} leading to increased intensity of EPR signal **I** **(***vide infra*). In summary, the initial addition of Mn^{2+} will lead to d-d emission along with a certain amount of broadening, the latter of which will decrease on further input of Mn^{2+} causing

simultaneously increased intensity and Mn^{2+}- Mn^{2+} pair formation with spin-orbit quenching of PL emission and exchange coupling being relevant to broad EPR lines as well as magnetic properties (*vide infra*).

3.4.3 Davydov splitting verified:

In order to prove the existence of Davydov type of interaction in the V_{Cd} emission at 2.25 eV we use our observation in Table 2 that the line width of this deconvoluted

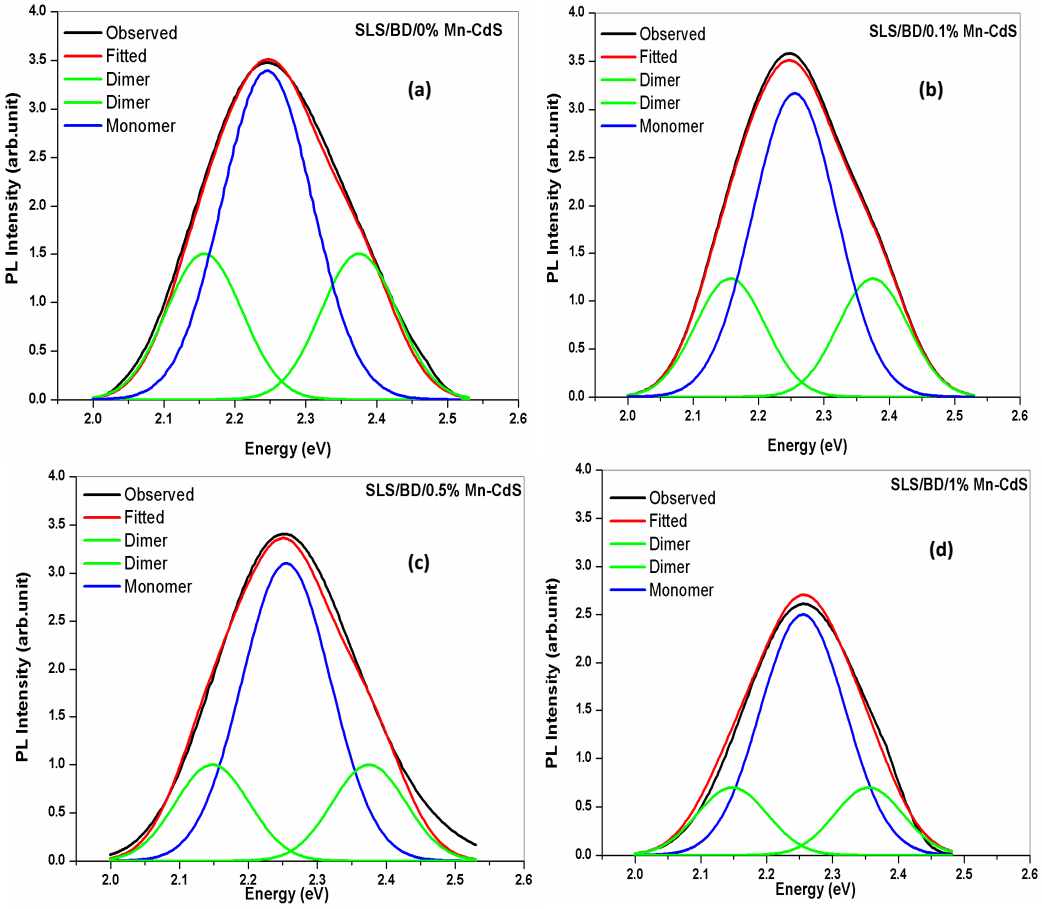

Fig. 4. Deconvolution of PL emission due to cadmium vacancies (V_{Cd}) in SLS/BD assisted CdS nanomaterials at different [Mn^{2+}] (a) 0%; (b) 0.1%; (c)0.5% and (d)1%.

emission drastically decreases from 1992 cm^{-1} to 1351 cm^{-1} with increase in concentration of Mn^{2+} from 0% to 5% . We have observed that this emission is caused by (i) both homometallic Cd^{2+}-Cd^{2+} vacant sites (ii) heterometallic sites of Cd^{2+}-Mn^{2+} pairs and (iii) isolated Cd^{2+} where the former will lead to unresolved Davydov split spectra and the latter two a single sharp line. We have *assumed* that the 5% Mn^{2+}/CdS contains only the latter two species, viz. isolated Cd^{2+} and possibly much less of Cd^{2+}-Mn^{2+} pairs

giving rise to a sharp single emission at 2.25 eV with a line width of 1351 cm^{-1}. Using this emission peak due to non-Davydov interaction, as a constant, a deconvolution of all the other V_{Cd} emission lines from CdS with 0%, 0.1%,0.5% and 1.0% Mn^{2+} obtained from Fig. 3 were performed, the results of which are shown in Fig. 4. This Figure and the Table 3 clearly reveals that the Davydov splitting is constantly at 0.22 eV i.e. 1773 cm^{-1} with reduction in intensity at increased [Mn^{2+}]. Such large splitting has been reported earlier.[19,20]

Table 3. Deconvolution parameters for SLS/BD assisted CdS nanomaterials at different [Mn^{2+}]

SLS/BD assisted Mn/CdS	Peak position (eV)	Peak width (cm^{-1})	Peak amplitude (a.u)	Peak intensity (a.u)
Pure CdS V_{Cd}	2.25			
Monomer	2.375	1350	3.4	2295
Dimer	2.154	1301	1.5	976
0.1% Mn/CdS V_{Cd}	2.25			
Monomer	2.379	1351	3.18	2147
Dimer	2.149	1301	1.25	813
0.5% Mn/CdS V_{Cd}	2.26			
Monomer	2.379	1351	3.1	2093
Dimer	2.149	1301	1.01	657
1% Mn/CdS V_{Cd}	2.26			
Monomer	2.379	1351	2.5	1689
Dimer	2.149	1301	0.7	455

*Dimer energy separation = 0.22 eV

3.4.4 Emission profile for SLS/PD assisted CdS/Mn^{2+}:

The photoluminescence data for the preannealed CdS/Mn^{2+} samples prepared from SLS/PD assistance are similarly interesting but with similarities and differences from those of SLS/BD. The similarity is in the energy of V_{Cd} emission(2.25 eV) and d-d emission (2.12 eV) of Mn^{2+} in cadmium vacant sites and also a reduction in the intensity and line width of the former, substantiating the fact (*vide supra*) that the dimeric V_{Cd} sites are present in plenty before the addition of Mn^{2+} ions entering the cadmium vacancy sites as shown in ESI Fig. 4. A difference is noted in the d-d emission in CdS/Mn^{2+} of SLS/PD

medium by way of simultaneous reduction both in its intensity and line width showing a quick and preferential formation of dimeric Mn^{2+}- Mn^{2+} in the Cd^{2+}-Cd^{2+} leading to spin-orbit quenching as opposed to an increase in the intensity of the d-d emission in SLS/BD preferring a single occupation of Mn^{2+} ions in the vacant Cd^{2+} sites. This difference is also manifested in the EPR of SLS/PD and SLS/BD as a function of [Mn^{2+}] (*vide infra*). The deconvolution indicating the presence of both these emissions are shown in ESI Fig. 4 and the parameters from such a deconvolution are shown in ESI Table 3. The V_{Cd} line width decreases from 2005 to 1734 cm^{-1} as a function of increasing [Mn^{2+}] along with the corresponding decrease in intensity much different from the case of SLS/BD assisted CdS/Mn^{2+} crystals. It is interesting to note that the line width and intensity decrease in the PL of CdS/ Mn^{2+} nanocrystals are 33% and 52% in SLS/BD medium while the same are only 15% and 20% in SLS/PD medium suggesting the presence of more homometallic Cd^{2+}-Cd^{2+} vacancy pairs in the latter than the former and hence quicker Mn^{2+}- Mn^{2+} dimer formation confirming the reduction in intensity of d-d emission both by way of spin-orbit quenching through dimer formation and much less number of isolated vacant Cd^{2+} sites. We can conclude that SLS/PD medium creates more defects in CdS nanocrystals than SLS/BD medium. The presence of more homometallic Cd^{2+}-Cd^{2+} vacancy pairs in SLS/PD than in SLS/BD assisted nanocrystals of CdS is due to higher amount of hexagonal character in the former (90%) than in the latter(81%) in the morphological distribution. This further proves that vacancies and the related optical and magnetic properties are from hexagonal crystals.

3.4.5 Davydov Splitting from V_{Cd} in SLS/PD medium:

Again a deconvolution of the V_{Cd} part of the spectrum from the SLS/PD assisted CdS/Mn^{2+} nanocrystals (ESI Fig. 5) was attempted in a manner similar to that adopted for SLS/BD assisted case to account for its decreasing line width as a function of increasing [Mn^{2+}]. Similar results were obtained with a Davydov splitting of 0.23 eV i.e.1854 cm^{-1} (ESI Table 4).

3.5 Annealing leads to Mn^{2+} ionic migration

As anticipated, annealing of nanocrystals from both SLS/BD and SLS/PD media indicates that there is ionic migration of Mn^{2+} to form dimeric manganese in addition to

the already existing such pairs due to the occupation of Cd^{2+}- Cd^{2+} vacant sites by the dopant ion as indicated by a study on 5% Mn^{2+}/CdS crystals leading to decreased V_{Cd} emission and d-d emission. The formation of more dimeric Mn^{2+}- Mn^{2+} is more evident in EPR results and magnetism.

3.6 EPR profile predicts low temperature ferromagnetism

The nature of the local lattice environment of the paramagnetic species in the nanocrystals can be deciphered by an analysis of the EPR spectra. Fig. 5 shows the EPR spectra of as-prepared SLS/BD and SLS/PD assisted samples of manganese doped CdS nanocrystals measured at room temperature (RT)**.** All the polycrystalline samples of CdS/ Mn^{2+} show a set of six sharp nuclear hyperfine line pattern (allowed transition, $\Delta m_I = 0$) corresponding to the hyperfine splitting from ^{55}Mn and a set of 5 doublets with very low intensity (forbidden transition, $\Delta m_I = \pm 1$) lying in between the six allowed lines and we call it as signal I. The presence of forbidden lines and a hyperfine coupling constant of $|A| \sim 68$ G (6.8 mT) indicates Mn^{2+} to be in a distorted tetrahedral crystal field environment.[21,22] In addition, there is a very broad line but low in amplitude caused by dipolar interaction and/or exchange-coupling due to nearby Mn^{2+}-Mn^{2+} dimers or clusters (call it, signal II) overlapping the sharp hextet as can be observed clearly in high percentage manganese doped CdS nanocrystals.

It is observed that the intensity of signal I due to isolated Mn^{2+} increases on increasing $[Mn^{2+}]$ in SLS/BD assisted nanocrystals, the reverse being the case for those from SLS/PD medium. But the signal II due to Mn^{2+}-Mn^{2+} interaction increases on increasing Mn^{2+} concentrations in both cases though the rapidity of increase in cluster formation is slower in the former and relatively faster in the latter. The agreement between the PL and EPR experimental findings confirms our interpretation as to the origin and emergence of both isolated Mn^{2+} from isolated Cd^{2+} and from heterometallic Mn^{2+}-Cd^{2+} sites and coupled Mn^{2+}-Mn^{2+} from coupled homometallic Cd^{2+}-Cd^{2+} sites. It is judiciously assumed that distantly separated Mn^{2+} ions may not give rise to any exchange and also the broadening contribution will be much less, being $1/r^3$ dependent.

We also like to explain why EPR spectra (Fig.5) of as-synthesized CdS/Mn^{2+} nanocrystals are so different when made from SLS/BD and SLS/PD. The nanocrystal

formation and its size are influenced both by surfactant and ligand, rate of formation of CdS/MnS as a function of the length of ligand L, rate of departure of the ligand and rate of nucleation to form crystals. The commonality is the surfactant but the ligands are different with BD being longer than PD. Hence, (i) the stability of CdL_2 complex is dependent on chelation ring size in CdL_2 with the bidentate ligands L, i.e. $Cd(ED)_2 > Cd(PD)_2 > Cd(BD)_2$ and consequently the reactivity with S^{2-} will increase in the reverse order resulting in fastest formation of CdS in BD medium; however, (ii) the departure of the longer bidentate ligand from Cd^{2+} will take a longer time through the solvent/surfactant barrier to facilitate the approach of S^{2-} to form CdS nanocrystals. In other words, the rate of departure of the ligand from Cd^{2+} plays a more dominant role than the chemical binding role in the CdL_2. Between these two factors the latter understandably is more important leading to faster nucleation to form crystals of SLS/PD medium than that of SLS/BD. Faster nucleation means more defects formation which is more true of SLS/PD and hence our above observation.

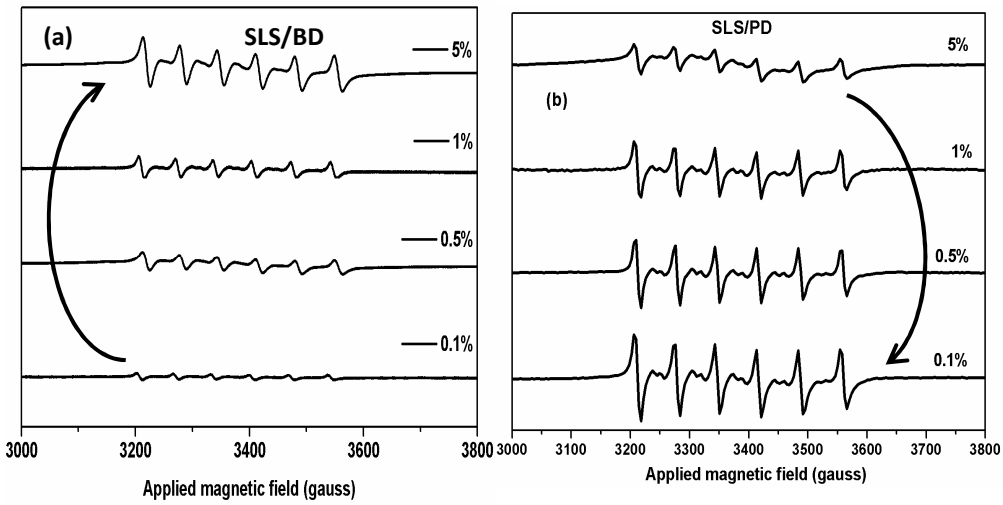

Fig. 5: EPR spectra of as-synthesized CdS/Mn^{2+} nanocrystals made from (a) SLS/BD and (b) SLS/PD media measured at room temperature

Furthermore in SLS/BD case, the intensity ratio of the broad line at RT and Liquid Nitrogen Temperature (LNT), I_{LNT} / I_{RT} (image of LNT not shown here) was found to be 8.8 for 5% Mn^{2+} doped pre-annealed sample; this substantial increase of intensity at low temperatures, more and above of what is estimated on the basis of pure Boltzmann population differences, predict strong cluster formation possibly in the form

of dimers resulting in ferromagnetic coupling, as suggested also by its origin from Davydov split dimers. This strong cluster formation is further confirmed by measuring their EPR at even lower temperature around 10 K (Fig. 6a and 6b) when the broad EPR line becomes even more intense at 10K. There is only a slight change in the line width of ~ 0.5mT on cooling to 10K for the pre-annealed sample, the actual line width being 41.7mT (at RT).

However, for those same clusters, the post-annealed samples exhibit a higher line width of 56.9 mT measured at both 300 K and 10 K for signal II, in addition to increased intensity. This increase for post annealed samples suggests the formation of more number of clusters with greater closeness during the annealing process resulting in both exchange plus dipolar interaction. But the simultaneous presence of isolated Mn^{2+} in both pre-annealed and post annealed nanocrystals also exhibit the same hyperfine value of ~ 6.8 mT in signal I at low temperatures indicating in no symmetry change.

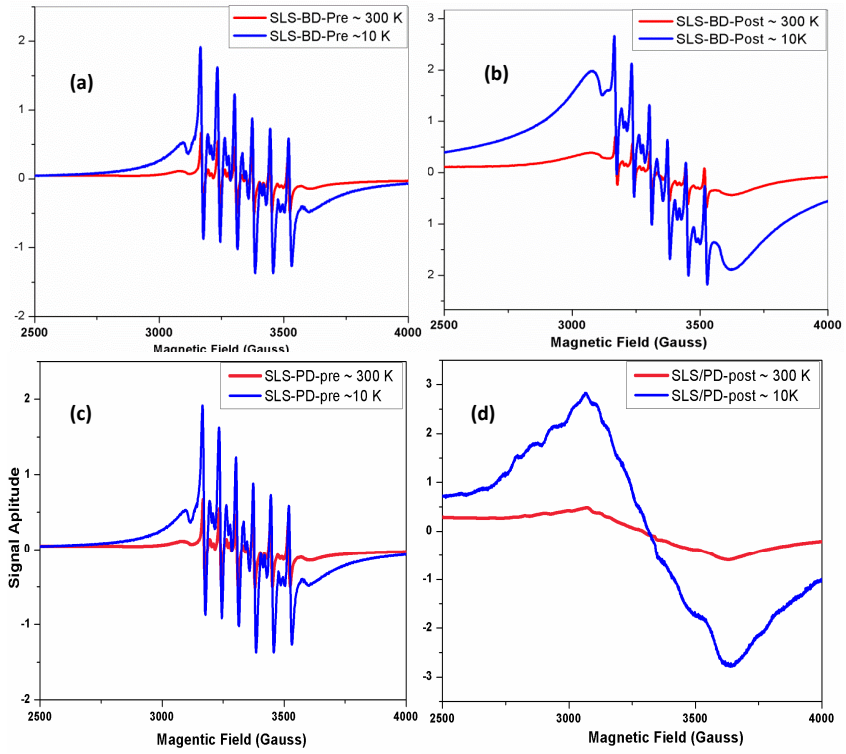

Fig. 6: EPR spectra measured at ~ 300 K and ~ 10 K for pre-annealed and post-annealed CdS/Mn^{2+} nanocrystals from SLS/BD (a and b) and for the same from SLS/PD medium(c and d)

In contrast to CdS/Mn^{2+} nanocrystals of SLS/BD, the crystals of pre-annealed and post-annealed crystals of SLS/PD origin exhibit a line width of ~ 52 mT (520 G) and ~ 57 mT (570 G) respectively with no temperature dependence as shown in Fig. 6c and 6d. Both the systems show an increased line width during the annealing process the increase is more substantial in the case of SLS/BD than in that of SLS/PD. This is in tune with the findings from PL studies which reveal the presence of more Mn^{2+}- Mn^{2+} dimer formation with SLS/PD assistance even during the initial addition of manganese as compared with SLS/BD assistance. Another interesting observation is almost the total suppression of signals due to isolated Mn^{2+} in post-annealed SLS/PD sample indicating a stronger ionic migration process in crystals of SLS/PD as compared to SLS/BD origin. Substantial line width increase in both post-annealed samples as compared to that of pre-annealed could be attributed to possible lattice contraction during the annealing process and more dimer formation due to ionic migration. But what is important to note is that though the temperature dependent EPR suggests ferromagnetism due to exchange coupled Mn^{2+}-Mn^{2+} dimers in the nanocrystals of CdS/5%Mn^{2+} from both SLS/BD and SLS/PD, differences in the temperature dependent EPR suggests more through finer details of their differing magnetic properties (*see next section*).

3.7 Magnetism in manganese incorporated CdS nanocrystals

3.7.1 Magnetism for SLS/BD assisted CdS/Mn^{2+}

The magnetic measurements for pre and post-annealed CdS/5%Mn^{2+} nanocrystals are shown in Fig. 7. The exact percentages of manganese concentration have been calculated from ICP-OES and they are found to be 4. 77%, 0.96%, 0.46% and 0.093% respectively for 5%, 1%, 0.5 % and 0.1% Mn/CdS of SLS/PD assisted nanocrystals, whereas, the corresponding values are 4.82%, 0.96%, 0.45% and 0.095% Mn/CdS of SLS/BD assisted nanocrystals. The typical M vs T curve for pre annealed sample shows a paramagnetic curve as the magnetic moment gradually increases on decreasing the temperature down to 5 K. This has been further confirmed by the magnetization measurement as a function of magnetic field, which exhibits typical paramagnetic behavior (linear curve) at higher temperatures; however, at very low temperature it

exhibits weak ferromagnetism[23], i.e., around 8 K it shows a small hysteresis curve with measurable values of coercivity (H_C) and remanence (H_R). On the other hand, the post-annealed 5% CdS/Mn^{2+} shows a small cusp around 30 K in the M *vs* T curve disclosing a transition point, i.e., Curie temperature (T_C) and a much different M *vs* H with a very prominent hysteresis curve below 60K. The measured coercive field (H_C) in pre-annealed and post annealed samples reveals maximum ferromagnetism at lower temperatures. For example, at 8 K, the measured coercivity (H_C) and remanence (H_R) for pre annealed and post annealed samples are 460 Oe, 2245 Oe and $0.06x10^{-4}$, $0.4x10^{-4}$ emu/g respectively, whereas at 20 K these values are much lower. The similarly

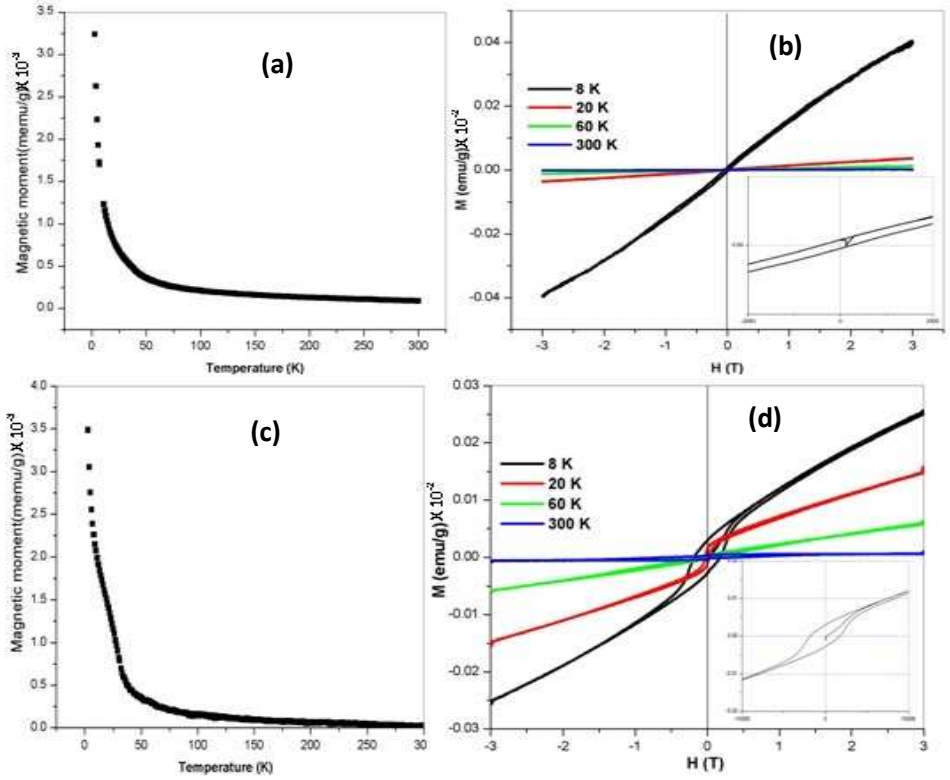

Fig. 7. Magnetic measurements of M vs T for (a) pre-annealed and (c) post annealed CdS/Mn^{2+} nanocrystals with the applied of 0.5T and M vs H curves (hysteresis) for (b) pre-annealed (d) post-annealed 5% CdS/Mn^{2+} nanocrystals at different temperatures. The inset shown in (b) and (d) are respectively the magnified region of pre and post annealed samples.

measured H_C and H_R values for the corresponding materials i.e. CdS/Mn^{2+} from CTAB/BD medium[12] at 8 K and 20 K are higher than those for materials of the current studies, despite having almost similar particle size obtained through same synthetic route but with a different surfactant, cetyltrimethylammoniumbromide, CTAB. The measured value of coercivity and remanence (H_R) at various temperatures are found in Table 4. In addition we observed no magnetic saturation (M_S) in all the cases even up to 3T and no saturation may occur even after applying higher field. This reveals the paramagnetic contribution being still present at all temperatures, in other words, while the coupled Mn^{2+} ions exhibit ferromagnetism the uncoupled Mn^{2+} caters to paramagnetism as can also be testified by the presence of hyperfine lines in EPR in both pre- and post annealed nanocrystals. Basically we have a case of simultaneous presence of exhibition of "ferromagnetism and paramagnetism". This may be due to the presence of a larger number of Cd^{2+} vacancies in the SLS/BD system.

Table 4. The measured magnetic values for pre and post annealed 5% CdS/Mn^{2+} nanocrystals of SLS/BD and (CTAB/BD*) origin.

5% CdS/Mn^{2+} Nanocrystals	Magnetism				
	T_C	H_C (Oe)		H_R (x 10^{-4} emu/g)	
		8 K	20 K	8 K	20 K
Pre-annealed	~ 35(35*)K	460 (2030*)	120(1800*)	0.01(7.6*)	-- (6.2*)
Post-annealed	~ 35(35*)K	2245 (2450*)	860(2330*)	0.04(13.8*)	0.03(10.5*)

A five-fold increase in coercivity after annealing is due to coupling of uncoupled Mn^{2+} by the ionic migration process to create more of coupled states as revealed also by an increase in EPR linewidth from 41.7mT to 56.9mT which itself could be due to lattice contraction.

3.7.2 Magnetism for SLS/PD assisted CdS/Mn^{2+} nanocrystals: Low temperature Ferromagnetism

The Zero-field cooling (ZFC) and Field-cooling (FC) magnetic profiles measured at 0.1T for pre and post annealed samples are shown in Fig. 8a. They show reversibility

in the ZFC and FC curves in both samples down to the temperature of 50 K representing its paramagnetic behaviour. However, below this temperature, a magnetic transition is observed in both samples around 35 K revealing the presence of ferromagnetism.[12] This is further confirmed by measuring hysteresis as a function of temperature. The pre-annealed sample shows a very low measured hysteresis value of ~ 410 Oe at 2 K. On the other hand, the post annealed sample shows a clear loop with measured hysteresis value of 1750 Oe at 2 K and the value is very low at 50 K as shown in Fig. 8(b). Coercivity has increased after annealing mostly due to ionic migration as seen in Fig. 8(c).

3.7.3 Ferromagnetism coupled SPM turns to Ferromagnetism on annealing

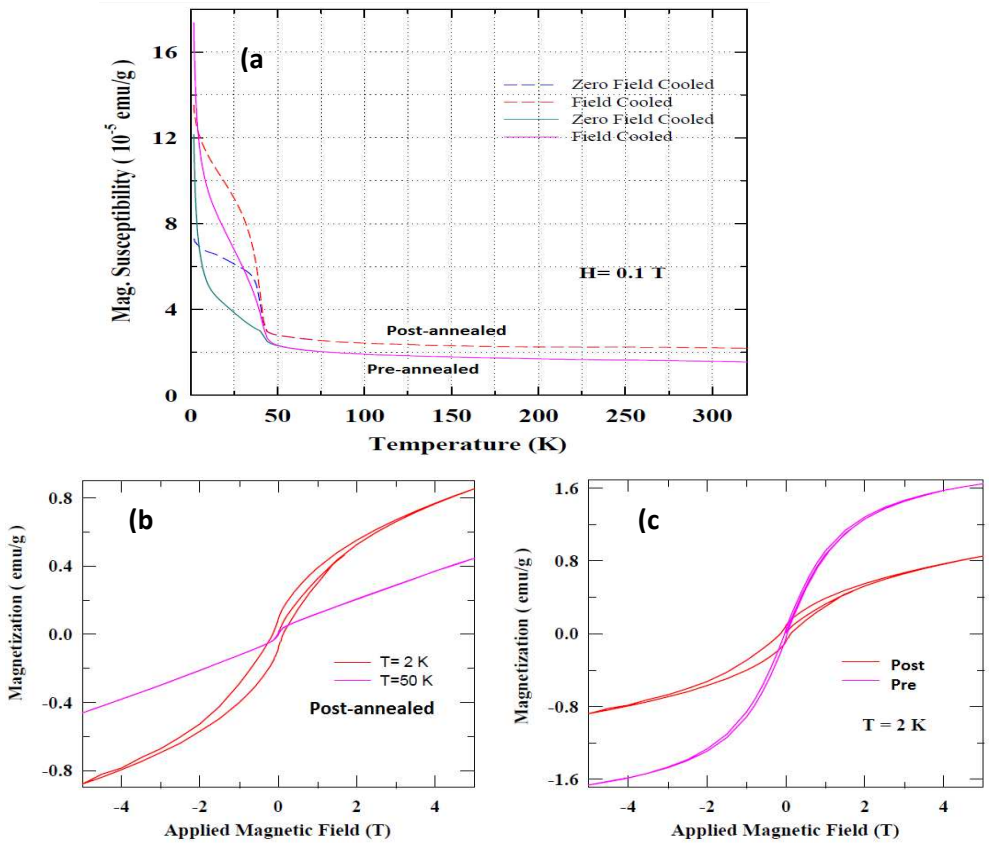

Fig. 8. (a) ZFC and FC measurements for SLS/PD assisted pre and post annealed samples of 5% CdS/Mn^{2+} nanocrystals with the applied magnetic field of 0.1 T; Hysteresis curves for (b) post-annealed sample at 50 and 2K; (c) comparison of pre and post annealed samples at 2 K.

If the size of the magnetic nanoclusters is in smaller size or in critical region, then they would have normally showed the superparamagnetic(SPM)[5,24] behavior with a low blocking temperature (T_B). The SPM behaviour can normally be identified by careful analysis of ZFC/FC curves. It is noteworthy that the ZFC/FC curves for both pre and post annealed samples exhibit reversibility down to the temperature at 50 K, below this temperature both materials show bifurcation in the ZFC and FC curves followed by sudden increase in their magnetic moment with cusp around 35 K. EPR spectra of pre-annealed SLS/PD at 10 K reveals the substantial presence of manganese hyperfine lines in addition to slight increase line width (from 52 to 57mT) along with an increase in intensity for the broadline probably indicating the simultaneous presence of ferromagnetism and superparamgnetism.[25] On the other hand the post annealed samples both at 300 K and 10 K show mainly a broad EPR line (with a small increase in linewidth on cooling) and with almost no presence of manganese hyperfine lines revealing it to be ferromagnetic. Hence the pre-annealed samples with smaller smaller particle size with low coercivity may represent the simultaneous presence of both superparamgnetism and ferromagnetism while ionic migration of Mn^{2+} on annealing provides for a transition from superparamgnetism to complete ferromagnetism.

3.8 Microscopy Analysis:

The high resolution transmission electron microscopy (HRTEM) of undoped CdS, 5% manganese doped CdS nanocrystals of SLS/BD and SLS/PD are shown in Fig. 9a, b and c respectively. The measured particle sizes are in the range of 5 to 15 nm in both SLS/BD and SLS/PD with no significant changes as function of doping concentrations but with a clear observation of lattice fringes. The measured lattice fringes are 0.33 and 0.32 nm respectively with SLS/BD and SLS/PD assisted 5% CdS/Mn^{2+} revealing the (002) plane of hexagonal phase as shown Fig. 9b and 9c and this is in accord with the dominant peak observed in XRD (Fig.1). The EDS profile of SLS/BD assisted 5% CdS/Mn^{2+} as shown in Fig.9d reveals serious cadmium deficiency, supporting the observation of the same by photoluminescence.

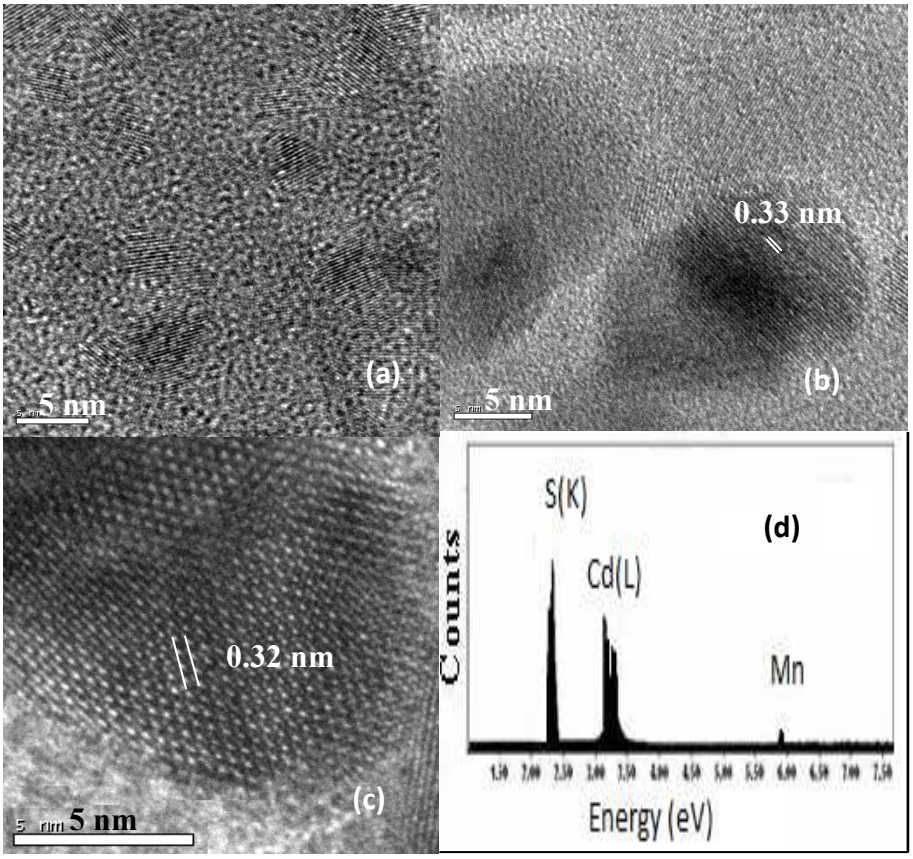

Fig. 9. The HRTEM images of SLS/BD assisted (a) pure (b) 5% manganese doped and (c) magnified particle image of 5% manganese doped SLS/PD assisted CdS nanocrystals, (d) EDS pattern for SLS/BD assisted 5% CdS/Mn^{2+} nanocrystals.

The magnified high resolution image of CdS/5%Mn^{2+}/PD nanocrystals as shown in Fig. 9c. A clear view of lattice fringes with measured d value of 0.32 nm confirms the (002) plane of hexagonal CdS. It is important to note that cadmium ion deficiency is quite high from the EDS, an inference well supported by photoluminescence spectroscopy and magnetism through EPR and magnetic measurements. It is interesting to note that the percentage of Cd in BD is higher than the PD reveals the Cd vacancies in SLS/PD assisted samples is higher than the corresponding SLS/BD assisted samples.

3.9 CdS and carbon nanoparticles (CNP) based Photovoltaic measurement

CdS is one among the best materials for photosensitivity[26] and its physico-chemical properties will be affected by particles size. The addition of CdS and other ions having unpaired elctrons to CNP , thereby creating heterostructures[27], could be a major advantage for enhancing photocurrent. Hence, we have tested the effect of Mn^{2+} additon by comparing un-doped CdS (SLS/BD/0%Mn), 5% Mn/CdS of SLS/BD and SLS/PD origin, added to CNP. The sythesis of Carbon nanoparticles (CNP) followed by earlier work[28], the detailed experiemental work and photocurrent set up (ESI Fig.6) are given in supporting file.

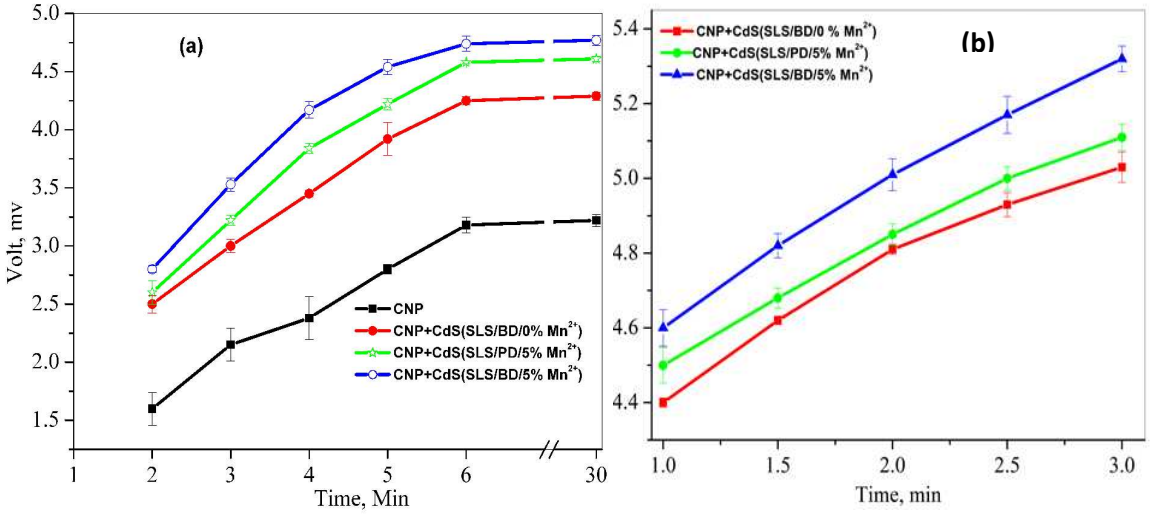

Fig. 10. Photovoltic profile (Voltage Vs Time) for (a) CNP and CdS/CNP heterostructures at 25 ºC (b) CdS/CNP heterostructures at 32 ºC.

The photosensitivity measurements for pure CNP as well as that of the heterostructures with CdS/ 0% and 5% Mn^{2+} of SLS/BD and SLS/PD origin at 25 ºC are shown in Fig. 10a. The voltage increases as a function of time of exposure to light in all cases. However, the latter samples show an enhancement in measured voltage over pure CNP. It is also interesting to note that 5%Mn/CdS of SLS/BD sample exhibits a slightly higher voltage followed by SLS/PD assisted 5%Mn/CdS and SLS/BD assisted pure CdS sample. In other words the increase in voltage follows the order: Pure CNP < CNP+ CdS < CNP+ CdS/5% Mn^{2+} (SLS/PD) < CNP + CdS/5% Mn^{2+}(SLS/BD). This trend can be

explained on the basis of high visible light absorption property. A look at the values of the band gap of these three materials along with that of CNP, is expected to follow the same trend as explained for similar materials with CNT (Carbon Nanotube). First of all it should be noted that the heterostructures mentioned here are similar to that of CNT/TiO_2 with metal ions like Pd(II), Ni(II) etc.,[29,30] with photon to electron conversion by promotion of valence band to the conduction band, i.e. the band gap energy[31]. However, the increase in band gap energy follows the order CdS/5% Mn^{2+}(SLS/BD) with 510 nm (2.43 eV) < CdS/0% Mn^{2+}(SLS/BD or PD) with 494 nm (2.51 eV) < CdS/5% Mn^{2+}(SLS/PD) with 488 nm (2.54 eV) as suggested by Fig.2. The reverse is true for transition probability. An illustration of electron hopping from CdS with CNT is given in Scheme I of Kim and Park[31]. The same holds good here with CNP.

Though this is an important factor another important factor also comes from vacancies of these materials which happen to switch the order of the latter two. It may be remembered that there is a decrease in vacancies in CdS/0% Mn^{2+}(SLS/PD or BD) > CdS/5% Mn^{2+}(SLS/PD) > CdS/5% Mn^{2+}(SLS/BD). This order is in correspondence to experimental observation of increasing voltage. These two competing factors played their roles in determining our experimental observation. Pure CdS possesses a large number of cadmium vacancies which can effectively trap the excited electrons from the conduction band and thus it has fewer number of free electrons responsible for the photosensitivity properties. It may be further pointed out that there is substantial increase in the voltage of three materials (CNP +CdS + Mn^{2+}) as compared to pure CNP. Manganese ions partially block the traps (being substituted in the cadmium vacancies) and hence enhance the prevention of electron-hole charge recombination.

The temperature dependent photo-resistance for CdS and CNP based heterostructures show increased voltage as a result of increasing resistance. The temperature dependent voltage at 25°C and 32 °C for the heterostructures of CdS/CNP samples is shown in Fig.10b. When connected in series of 4 cells, voltage increases with time of exposure at 32°C from 4.4 to 5.03 mv, for SLS/BD assisted pure CdS sample (Fig. 10b) over 3 minutes of exposure to light. The same increase at 25°C is from 2.5 to 3

mv at the same time of exposure; however, its reaches 4.25 mv in 6 mins. The measured voltage for 5% Mn/CdS of SLS/BD and SLS/PD assisted samples are 4.6 to 5.32 and 4.5 to 5.11 mv respectively for the same time of exposure. It is easily seen that an increase in the temperature of the sample at all times gives a higher voltage though the rate of increase is a little lower at higher temperature. However, on increasing the exposure time to 30 mins at a given temperature the voltage becomes a plateau in all the samples (Fig. 10a). The measured voltage of CdS/CNP thermistor is proportional to the visible light intensity and temperature.

4. Conclusion

CdS and manganese doped CdS have been made by a simple wet chemical route with two different ligands using a single surfactant, SLS, in this work. The samples from SLS/BD and SLS/PD assisted preparations show that the hexagonal phase predominates over cubic phase. The UV-Visible study shows red and blue shifts respectively in their band gap positions as function of [Mn^{2+}] of SLS/BD and SLS/PD assisted CdS/Mn^{2+} nanocrystals accompanied by reversing intensity changes. The best part of the current work is the finding of Davydov split PL emissions originating from the nearby but interacting cadmium ion vacancies; however, when they are filled up subsequently by manganese ions a difference is noted in the magnetic properties of samples of BD and PD origin. But the commonality is the observation of ferromagnetism, though of differing magnitude, after the samples are annealed indicating ionic migration. Another interesting aspect is that these nanoparticles when combined with CNP could act as good thermistors.

Acknowledgements

PTM acknowledges the SERB, DST, Government of India for research scheme (SR/S1/IC-53/2012). He also thanks the INSA for a Senior Scientistship. SA acknowledges the DST and UGC, New Delhi for the financial support. BS acknowledges CSIR for Senior Research Fellowship and IIT/Madras for an Institute Post-doctoral Fellowship. We thank Professor S V Bhat, IISc Bangalore, for some EPR measurements.

Notes and References

1. E. L. Brus, *Appl. Phys*. *A*, 1991, **53**, 465-474

2. H. Weller, *Angew. Chem. Int. Ed. Engl.,* 1993, **32**, 41-53

3. P. K. Sharma, R. K. Dutta, R. J. Choudhary and A. C. Pandey, *CrystEngComm.*, 2013,**15**, 4438-4447

4. D. J. Norris, N. Yao, F. T. Charnock and T. A. Kennedy*, Nano Lett.,* 2001, **1**, 3-7

5. B. Sambandam, N. Rajendran, M. Kanagaraj, S. Arumugam and P. T. Manoharan, *J. Phys. Chem. C*, 2011, **115**, 11413-11419

6. Y. Yang, O. Chen, A. Angerhofer, Y. C. Cao, *Chemistry*, 2009, **15**, 3186-97

7. X. Yuan, J. Zheng, R. Zeng, P. Jing, W. Ji, J. Zhao, W. Yang and H. Li, *Nanoscale***,** 2014, **6**, 300-307

8. X. Ji, H. Li, S. Cheng, Z. Wu, Y. Xie, X. Dong, P. Yan, *Mater. Lett.,* 2011, **65**, 2776–2778

9. Y. Shan, J. –J. Xu and H. -Y. Chen, *Chem. Commun.*, 2010, **46**, 4187-4189

10. F. Acomia, I. Salaorua, N. Apetroaeia, A. Vasileb, C. M. Teodorescuc and D. J. Macovei, *Optoelectron. Adv. Mater.,* 2006, **8**, 26

11. B. Sambandam and P. T. Manoharan, *J. Phys. Chem. C*, 2009, 113, 9486-9496

12. B. Sambandam, R. J. V. Michael, N. Rajendran, S. Arumugam and P. T. Manoharan, *J. Nanopart. Res*., 2012, **14**, 1067

13. B. Sambandam, S. Esaki Muthu, S. Arumugam and P. T. Manoharan, *RSC Adv.,* 2013, **3**, 5184-5195

14. M. A. Short and E. G. Steward, *Am. Mineral,* 959, **44**, 189

15. A. D. Arulsamy, U. Cvelbar, M. Mozetic and K. Ostrikov, *Nanoscale*, 2010, **2**, 728-733

16. A. Nag, R. Cherian, P. Mahadevan, A. Venu Gopal, A. Haz- arika, A. Mohan, A. S. Vengurlekar and D. D. Sarma, *J. Phys. Chem. C,* 2010, **114**, 18323-18329

17. A. Hazarika, A. Layek, S. De, A. Nag, S. Debnath, P. Mahadevan, A. Chowdhury and D. D. Sarma, *Phys. Rev. Lett.,* 2013, **110**, 267401

18. O. Chen, D. E. Shelby, Y. Yang, J. Zhuang, T. Wang, C. Niu, N. Omenetto and Y. C. Cao, *Angew. Chem. Int. Ed.*, 2010, **49**, 10132-10135

19. B. Birkan, D. Glen and Serdar zelik, *J. Phys. Chem. B*, 2006, **110**, 10805-10813

20. J. Takeda, S. Shinohara, N. Eguchi, S. Ohishi, S. Kurita and T. Kodaira, Proceedings of the 3rd International Conference on Excitonic Processes in Condensed Matter, ed. R. T. Williams and W. M. Yen ,The Electrochemical Society, Pennington, 1998, pp.135-140.

21. M. Azad Malik, P. O'Brien and N. Revaprasadu, *J. Mater. Chem.*, 2001, **11**, 2382-2386

22. S. Liu and X. Su, *Anal. Methods,* 2013, **5**, 4541-4548

23. S. Bhattacharyya, Y. Estrin, D. H. Rich, D. Zitoun, Y. Koltypin and A. Gedanken, *J. Phys. Chem. C,* 2010, **114**, 22002–22011

24. F. Zhan and C. Y. Zhang, *J. Mater. Chem.,* 2011, **21**, 4765-4767

25. Q. Li, Y. Wang, L. Fan, J. Liu, W. Kong and B. Ye, *Scripta Materialia,* 2013, **69**, 694-697

26. J. S. Jie, W. J. Zhang, Y. Jiang, X. M. Meng, Y. Q. Li and S. T. Lee, *Nano Lett.*, 2006, **6**, 1887-1892

27. Y. K. Kima and H. Park, *Energy Environ. Sci.,* 2011, **4**, 685-694

28. T. Muthukumar, S. Prabhavathi, M. Chamundeeswari, T. P. Sastry, *Materials Science and Engineering: C*, 2014, **36**, 14-19

29. L. Sheeney-Haj-Khia, B. Basnar and I. Willner, *Angew. Chem., Int. Ed.,* 2005, **44**, 78

30. I. Robel, B. A. Bunker and P. V. Kamat, *Adv. Mater.,* 2005, **17**, 2458

31. Y. K. Kim and H. Park, *Energy Environ. Sci.,* 2011, **4**, 685–694